Report no. changed (Mar 2006): SM-214-UU

SACLANTCEN MEMORANDUM
serial no.: SM-214

SACLANT UNDERSEA
RESEARCH CENTRE

MEMORANDUM

Extended towed-array processor by overlapped correlator

S. Stergiopoulos
and E.J. Sullivan

November 1988

Report no. changed (Mar 2006): SM-214-UU

Page count for SM-214
(excluding covers)

Pages	Total
i–vi	6
1–32	32
	38

SACLANT Undersea Research Centre
Viale San Bartolomeo 400
19026 San Bartolomeo (SP), Italy

tel: 0187 540 111
telex: 271148 SACENT I

NORTH ATLANTIC TREATY ORGANIZATION

SACLANTCEN SM-214

Extended towed-array processor by overlapped correlator

S. Stergiopoulos and E.J. Sullivan

The content of this document pertains to work performed under Project 02 of the SACLANTCEN Programme of Work. The document has been approved for release by The Director, SACLANTCEN.

Issued by:
Systems Research Division

J. Marchment
Division Chief

intentionally blank page

Extended towed-array processor by overlapped correlator

S. Stergiopoulos and E.J. Sullivan

Executive Summary: High bearing resolution in sonar systems becomes more important and more difficult to achieve, as the frequency regime is made lower to increase the range of detection. Since the range limiting noise is then essentially traffic noise, the angular separation of sources means increase of detection range. The requirement of larger arrays to provide higher low frequency bearing resolution leads to serious technical and operational implications.

The present investigation deals with the attempt to increase the effective length of a given array by synthesizing additional hydrophones. The techniques for extended angular resolution of a receiving array, the so-called synthetic aperture techniques, have been successfully applied in aircraft and satellite active radar systems. Applications of the above techniques to sonar systems have not been successful because of the presence of disturbed motion of the towed array by currents and the poor coherence of the acoustic signal in the sea as compared to the electromagnetic waves in the air.

The present approach in developing an algorithm to overcome the prohibitive impact is called 'extended towed-array processing'. The basic idea is a phase correction factor that is used to combine successive measurements of the moving towed array coherently to extend the effective towed array length. The decisive phase correction factor is derived by cross-correlating successive hydrophone signals of the array that overlap. Because of the temporal and spatial ovelapping, the algorithm properly compensates for the phase fluctuations of the received signal caused by irregularities of the tow path of the physical array and the acoustical propagation characteristics. As a result it is not necessary to have accurate estimates of the source frequency as is required by previous techniques.

The developed algorithm of extended towed-array processing has been successfully applied on synthetic data including types of errors that could exist in real measurements. Current efforts with real data are very encouraging and future plans include detailed experimental investigations to explore the merits of the new algorithm.

intentionally blank page

Extended towed-array processor by overlapped correlator

S. Stergiopoulos and E.J. Sullivan

Abstract: The development of an algorithm for extended towed-array measurements, which could be used by matched-field estimators to obtain information about depth and range of a source, is studied. This algorithm combines coherently the acoustic signal arrivals at a moving hydrophone towed array by making proper compensation through a phase correction factor for considerable fluctuations in phase, irregularities in the tow path of the physical array, as well as in amplitude during the coherent integration time. The concept of the extended towed-array processing is based on what we call overlapped correlator, which provides the phase correction factor by correlating overlapping space samples of the acoustic signal received at successive moments in time by the moving towed array. The algorithm has been applied on numerical data generated by the SNAP normal mode model. The effects of space and time coherence of the signal and the random and systematic errors on the extended towed-array measurements are examined and give guidelines for experimental applications of this algorithm.

Keywords: coherence ○ conventional beamformer ○ extended towed-array processing ○ matched-field estimators ○ maximum entropy beamformer ○ maximum likelihood beamformer ○ overlapped correlator ○ SNAP normal mode model ○ synthetic aperture ○ variance of estimates

Contents

1. Introduction

Improved processing performance for passive localization of a source in a waveguide, by including environmental information, has received increasing attention in recent years. The techniques involved in these processing schemes utilize measured data from a vertical [1–4] or horizontal [5] hydrophone array in conjuction with a propagation model and are called 'matched-field processing techniques'. An overview of related studies can be found in [6].

In general, the range/depth localization problem, which includes matched-field processing, matches the measured pressure field at the hydrophone array with theoretical estimates from the normal-mode propagation model of the expected field for source locations. These theoretical estimates are solutions of the wave equation, for the shallow-water case, at all array elements and for all possible point-source locations.

Experimental studies in matched-field processing, carried out in shallow water, include mainly field measurements from a vertical array. The main emphasis in the above studies [7–9] is related to the great difficulties in maintaining the hydrophone array vertical and straight during the experiment because of currents. As a result, the matched field results failed to produce an experimental solution when the vertical array was deformed or tilted. These effects of a deformed vertical array have been also demonstrated by numerical simulations [8].

The use of horizontal arrays to obtain estimates of depth and bearing for a source in a shallow waveguide has been suggested by Hinich [5] as being the configuration that provides the maximum information as an array design. Other investigators [10–12] have also studied the use of a towed array, which has more potential for practical applications, for source-location information. In a 'matched-field estimator' the horizontal field samples from a towed array are spatially spectrally analysed by a 'beamformer', from which the wavenumbers associated with a normal-mode model are estimated. The nature of the above estimates requires that the bearing of the source must be at endfire because the horizontal arrays cannot be used in broadside for range and depth estimation because of the fact that at broadside the modal arrivals differ only in amplitude but not in phase. Information regarding the horizontal component of the modal wavenumbers is thus not available.

It has been suggested by several numerical studies [11,13], however, that for a shallow-water waveguide the aperture of the horizontal field samples must be larger than 1 km in order to achieve the required wavenumber resolution for reasonably accurate source-location estimates. This restriction on the aperture size of the towed-array measurements poses a serious and practical operational problem.

In this memorandum, an attempt is made to provide an algorithm for extended towed-array measurements that achieves a desired aperture size using a 32-hydrophone array (i.e. 130 m). The algorithm should coherently combine the acoustic signal arrivals at a hydrophone array while making proper compensation for considerable fluctuations in phase, irregularities in the tow-path of the physical array, as well as in amplitude during the coherent integration time.

The techniques for extended angular resolution of a small receiving array, the so-called synthetic-aperture techniques, have been successfully applied in aircraft and satellite active-radar systems. Applications of these techniques to sonar systems [14,15] have tended to take directly the results developed for radars. Limitations, however, upon the length of a synthetic aperture using the above techniques were apparent because of the presence of tow-path and ocean-ray-path instabilities and the slow acoustic propagation velocity in water as compared to the electromagnetic velocity in air. Recent studies [16,17] have indicated that prospects for extended towed-array measurements appear to be sufficiently improved. Estimates of the space and time coherence of acoustic transmissions indicate phase shifts smaller than 180° for 20-min intervals and that the tow-path irregularities could approximately be controlled.

Our attempt to develop an algorithm for extended towed-array measurements that provides horizontal field samples for a matched-field estimator differs from previous techniques in the following:

- The bearing of the source is at the endfire of the towed array during the coherent integration time.
- During the integration period and between two successive sets of measurements with the moving towed array there are hydrophone samples that overlap.
- The averaged value of crosscorrelation estimates between the overlapped hydrophones provides the phase correction factor that is used to combine coherently the successive measurements of the moving towed array.
- This estimate of the phase correction factor for extended towed-array processing is a first-order prediction of what we call the 'overlapped correlator', and because of the overlapping process it is not necessary to have accurate estimates of the source's frequency as have been required by previous techniques.
- Errors associated with phase variations occurring during the coherent extension of the towed-array measurements are directly compensated for by the overlapped correlator since the phase correction factor is estimated from the horizontal field samples.
- The sea area for surveillance is shallow – about 10 to 20 wavelengths deep.

In this report a brief theoretical description of the horizontal field samples for the matched-field estimator derived from the extended towed-array processing by overlapped correlator is included. In Sect. 3 we discuss the processor design together with the synthesis of numerical data, which are used in this study as simulated experimental measurements to test the method. In the same section the error analysis is included and the effects of the time and space coherence during the coherent integration of the extended towed-array processing are examined. The results of the studies with simulated data are presented in Sect. 4, and a discussion of the application of the overlapped correlator in matched-field estimators is given in Sect. 5.

2. Theory

In matched-field estimators the propagation characteristics of the stratified waveguide are described by the normal-mode propagation model. In our application we consider the sound pressure field caused by a stationary point source in a shallow sea to be the summation of modes and this implies that the sea bottom at the surveillance area of concern must be approximately flat.

The analytic expression for the sound pressure field for the equally-spaced samples, at each hydrophone of the receiving array at range r_0 and depth z, and a source at depth z_0, is

$$P(r_n, z, t_i) = \exp[-j\omega t_i] \sum_{m=1}^{M} \Phi_m(z)\Phi_m(z_0) \frac{\exp[-\alpha_m r_n]}{\sqrt{k_m r_n}} \exp[j k_m r_n], \qquad (1)$$

where $r_n = r_0 + (n-1)d$ and $n = 1, 2, \ldots, N$ (n is the index of the nth hydrophone of the N-element towed array, d the spacing between the equally-spaced hydrophones in the towed array, $P(r, z)$ the acoustic pressure field), $t_i = i\Delta t$ and $i = 1, 2, \ldots, L$ (L is the number of data points of the pressure time series, Δt the sampling interval in time domain), $\Phi_m(z)$ the mth modal function evaluated at z, k_m the horizontal wavenumber for the mth mode, α_m the decay constant for the mth mode and M the number of modes supported by the propagation channel.

The above expression is the solution of the cylindrical wave equation that describes the pressure field. Estimates for the parameters $(\Phi_m(z), k_m, \alpha_m, m = 1, 2, \ldots, M)$ are provided by the SNAP model (i.e. SACLANTCEN's normal-mode model) [18].

In our numerical study, we have considered a set of boundary conditions that describe a shallow channel of 103 m depth, which is located in the Mediterranean just north of Elba. The bottom in this area is sufficiently flat and the synthetic data, generated by the SNAP model, describe very precisely the actual acoustic pressure field. The signal is generated by a source that excites the acoustic field in the above waveguide with narrowband energy at frequency ω. Later in this study we examine the effects of a finite bandwidth on the extended towed-array processing.

For a source at a horizontal range of 5 km and depth of 50 m the output from each sensor n (i.e. $n = 1, 2, \ldots, N$ and $N = 32$) of a 32-hydrophone array filtered in a narrowband about ω is given by Eq. (1). The towed array is at a depth of 50 m. Estimates for $\Phi_m(z), k_m$ and α_m are provided by the SNAP model. The number of normal modes M, according to the model, that describe the sound propagation for a frequency of 190 Hz is 9. For this numerical experiment the spectrum of the horizontal wavenumbers k_m is presented in Fig. 1 as derived from $P(r, z)$ in Eq. (1).

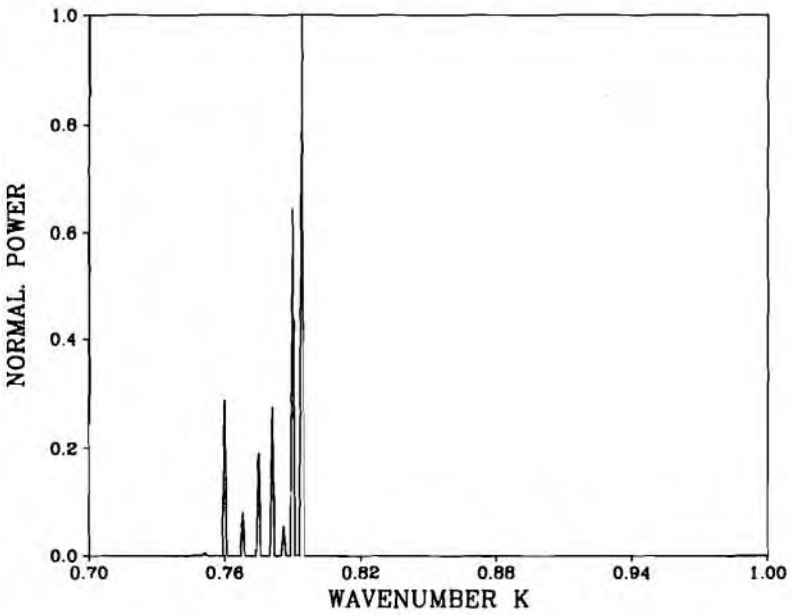

Km	Nor. Pow.
0.7500	0.0041
0.7590	0.2865
0.7670	0.0802
0.7740	0.1917
0.7800	0.2756
0.7850	0.0552
0.7890	0.6429
0.7910	0.0005
0.7930	1.0000

Fig. 1. The spectrum of horizontal wavenumbers k_m, computed from the SNAP model which characterize the sound propagation for a frequency of a source 190 Hz and at a depth 50 m. The receiving array is at 50 m depth and horizontal range 5000 m. The depth of the sea is 103 m.

As expected, the wavenumber spectrum is different for a situation where the towed array is at a depth of 50 m and the source at 35 m, as can be seen in Fig. 2.

Our goal in this study is to recover the wavenumber spectrum from the horizontal field samples of a 32-hydrophone receiver through extended towed-array processing. As was mentioned in the introduction, the concept of extended towed-array processing to achieve high-resolution beamforming for the k_m spectrum is based on what we call the 'overlapped correlator'. In other words, during the passive mode of operation there are space samples of the acoustic signal, received at successive positions by the moving towed array, that overlap. The averaged value of crosscorrelation estimates between the space samples of the overlapped hydrophones provides the phase correction factor, which is a phase compensator for the delay time and the movement of the towed array between samples. This phase correction factor is used to extend the towed-array space measurements. This concept is illustrated in Fig. 3, where we have the successive positions of the receiving array in terms of time and hydrophone spacing.

Let us assume v to be the speed of the towed array moving along the axis which coincides with the bearing of the source. At time $t = 0$, we sample the acoustic

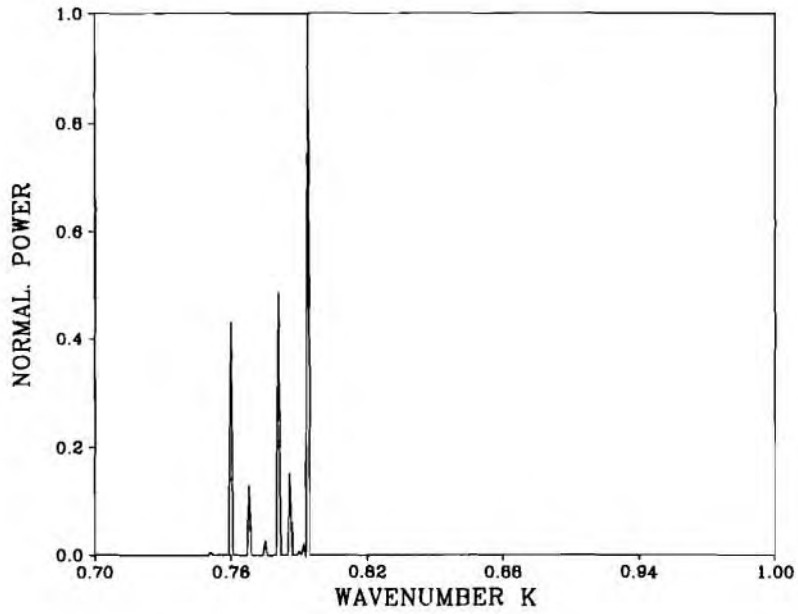

Fig. 2. The spectrum of horizontal wavenumbers k_m which describe according to the SNAP model the sound propagation for the same parameters as in Fig. 1 except that the source is at 35 m depth. The difference between Figs. 1 and 2 is on the relative size of the normalized power of k_m. This difference indicates how the spectrum of k_m is viewed from the receiving towed array when the source is at different depths.

pressure field with the receiving N-element towed array. At time $t = \tau$ the array has moved by τv and by proper choice of the parameter v we have $\tau v = qd$, where q represents the number of hydrophone positions that the towed array has moved. In Eq. (1) we change t_i to t_{li}, where l represents the lth set of measurements in time. The parameter J (i.e. $l = 1, 2, \ldots, J$) gives $T = J\tau$, the integration period of the extended towed-array processing. Also in Eq. (1) the parameter r_n is modified to r_{ln}, where

$$r_{ln} = r_0 + (lq + (n-1))\, d, \quad n = 1, 2, \ldots, N. \tag{2}$$

As shown in Fig. 3, between two successive set of measurements (i.e. l, $l+1$) there are $(N - q)$ samples of the acoustic pressure field that represent the same position in space but differ in time by the factor $\exp[j\omega\tau]$. Hence, for this set of samples the acoustic pressure field according to Eq. (1) at the time moment t_{li} is

$$P(r_{ln_0}, z, t_{li}), \quad n_0 = q+1, q+2, \ldots, N, \tag{3}$$

and at the time moment $t_{(l+1)i}$ it is

$$P(r_{(l+1)n}, z, t_{(l+1)i}) = \exp[-j\omega\tau] P(r_{ln_0}, z, t_{li}), \quad n = 1, 2, \ldots, N-q. \tag{4}$$

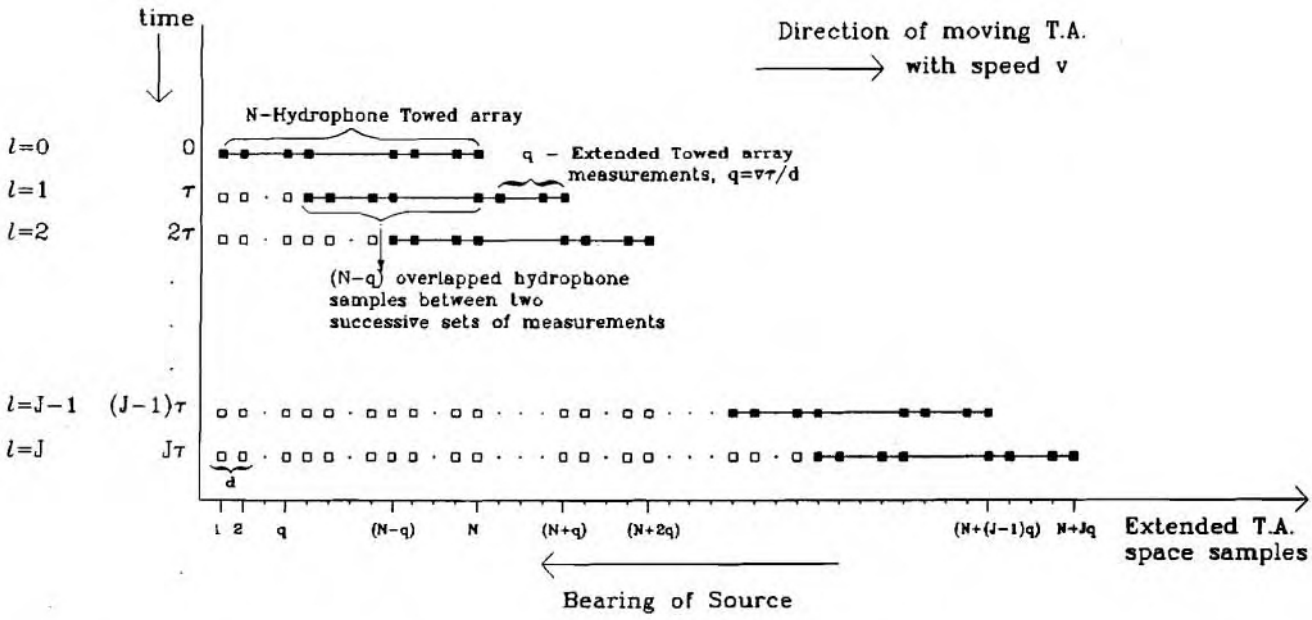

Fig. 3. **Configuration of the $(N + Jq)$ extended towed-array space samples based on the integration from an N-hydrophone towed array; successive set measurements.**

Then the phase term that includes all the effects caused by the delay time and movement of the receiving array is given by

$$\Psi(\omega\tau)_y = \arg[P(r_{ln_0}, z, t_{li})|P^{\dagger}(r_{(l+1)n}, z, t_{(l+1)i})]_y, \quad y = 1, 2, \ldots, N-q, \tag{5}$$

where † denotes complex conjugate.

As a result of Eq. (5), an estimate of the phase correction factor is given by

$$\tilde{\Psi}(\omega\tau) = \frac{1}{N-q}\sum_{y=1}^{N-q}\Psi(\omega\tau)_y. \tag{6}$$

The $P(r_{ln}, z, t_{li})$ for $n = 1, 2, \ldots, N$ samples of the acoustic pressure field could be extended by q more samples, based on the modification of the next set of measurements, as follows:

$$P(r_{ln_0}, z, t_{li}) = \exp[j\tilde{\Psi}(\omega\tau)]P(r_{(l+1)n}, z, t_{(l+1)i}), \tag{7}$$

where $n_0 = N+1, N+2, \ldots, N+q$ and $n = N-q+1, N-q+2, \ldots, N$.

In the same way the first set of N samples of the N-element receiving array could be extended during the integration period $T = J\tau$ by measurements (Jq) so that the total number of space samples is $N + Jq$, which could be a preselected desired number.

When idealized parameters are assumed, the expected value of the phase correction factor [14,15] in Eq. (5) is

$$\tilde{\Psi}(\omega\tau) = \omega\tau. \tag{8}$$

There are, however, many types of errors, which are examined in the next section, and their effects determine the optimum (or maximum) length of the extended towed-array measurements. At this point we assume the effects of errors in Eq. (8) to be random noise with zero mean and variance σ_y^2. Then the phase correction factor could be expressed by

$$\Psi(\omega\tau)_y = \tilde{\Psi}(\omega\tau) + \epsilon_y \tag{9}$$

and an estimate of $\tilde{\Psi}(\omega\tau)$ is derived in the least-squares sense by minimizing

$$\sum_{y=1}^{N-q}(\Psi(\omega\tau)_y - \tilde{\Psi}(\omega\tau))^2 = \min. \tag{10}$$

The solution of the above least-squares problem is given by Eq. (6). This rather simplistic treatment of the errors, by assuming ϵ_y to be random noise, has been successfully applied in our error analysis where random and systematic errors are considered. The application, however, of our algorithm in real data could reveal whether the above assumption about errors in Eq. (9) is sufficient. This, of course, would require a specific model of the noise when determining $\tilde{\Psi}(\omega\tau)$ by the minimization of Eq. (10).

3. Numerical experiment

As mentioned in the previous section, the extended towed-array processing scheme has been tested with numerical data generated by the SNAP model based on a location in the Mediterranean just north of Elba. In this section we present the processor design of the extended towed-array processing and examine the effects of random and systematic errors on the extended towed-array samples.

3.1. PROCESSOR DESIGN

Following the presentation of the concept of the extended towed-array processing by overlapped correlator, we present the processor design of this concept which is illustrated in Fig. 4. At this point we consider it appropriate to mention a few points regarding the processing steps shown in the schematic diagram of the above figure.

- The overlap size of the hydrophone space samples between two successive sets of measurements was chosen to be 75% of the N-element towed array. Later in this paper we examine the effect of the overlap size on the extended towed-array measurements.
- There is a better estimate in recovering the wavenumber spectrum of k_m by correlating overlapped measurements between $l = g$ and $l = g+1, l = g+2, l = g+3$ experimental runs than correlating between successively overlapped set measurements (i.e. $l = g$ and $l = g + 1$, $l = g + 1$ and $l = g + 2$, etc.). Following the first approach (i.e. overlapped correlation between $l = g$ and $l = g + 1, l = g + 2, l = g + 3$) the phase correction factor is derived between the first experimental run and the following set of measurements so that the computational round-off errors, which propagate between the successive calculations in the overlapped correlator, are reduced as much as possible.

Recovery of the k_m spectrum is obtained by beamforming the extended towed-array measurements. Shown in Fig. 5 is the k_m spectrum, derived by applying conventional beamforming from synthetic data generated by the SNAP model. The signal-to-noise ratio is infinite. The value of the parameters, defined in Sect. 2, with respect to the extended towed-array processing, is also shown. In the same figure we have the results by beamforming the field samples from an actual 512-hydrophone towed array in comparison with the results derived by beamforming the 512-extended towed-array samples, where the samples have been obtained from a 32-hydrophone towed array moving with a speed of 2.5 m/s (i.e. 4.8 kn). Here it is seen that there is no difference between the two cases, and this is a demonstration of how insensitive the technique is to the computational round-off errors.

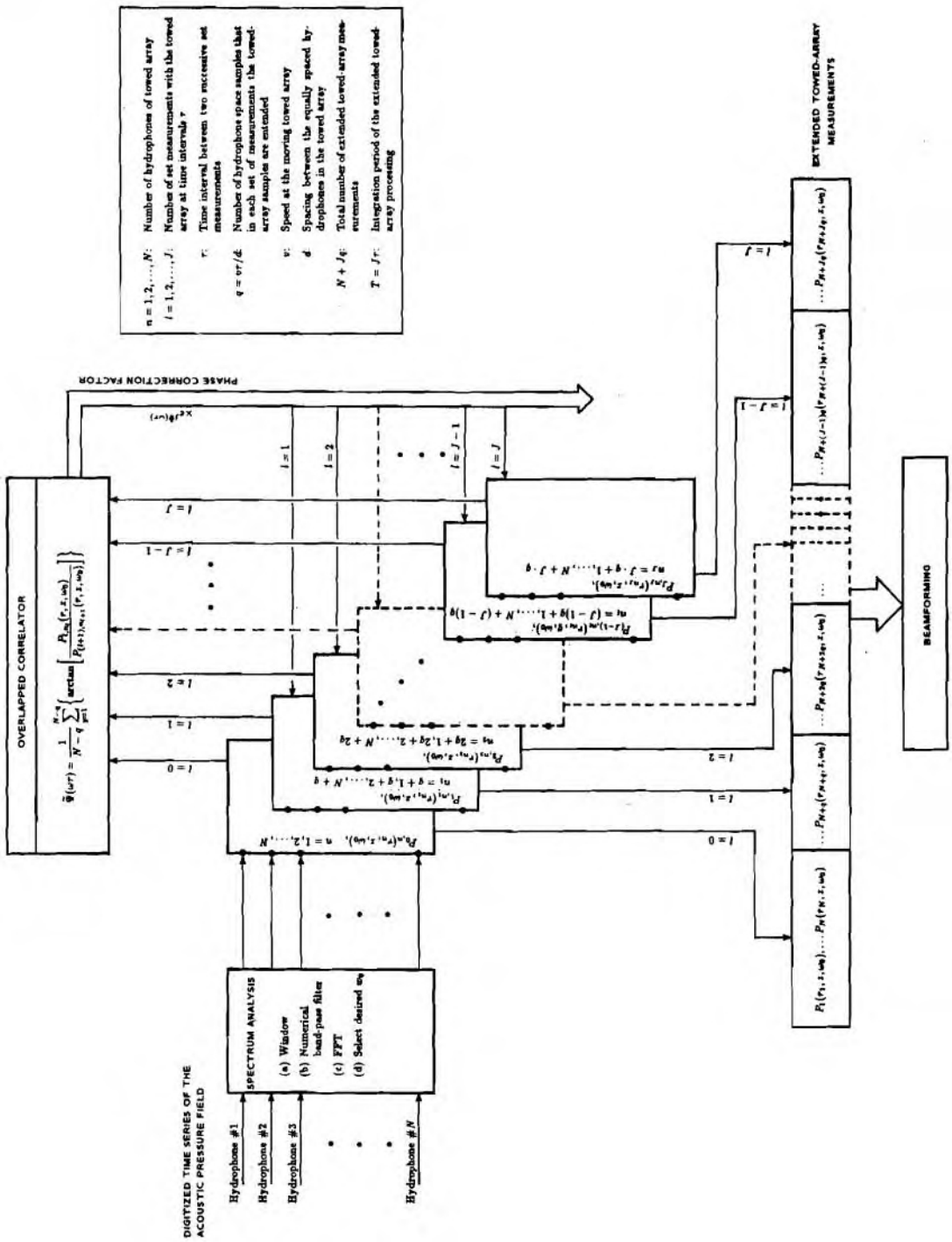

Fig. 4. Schematic of the processor design regarding the extended towed-array processing by overlapped correlator.

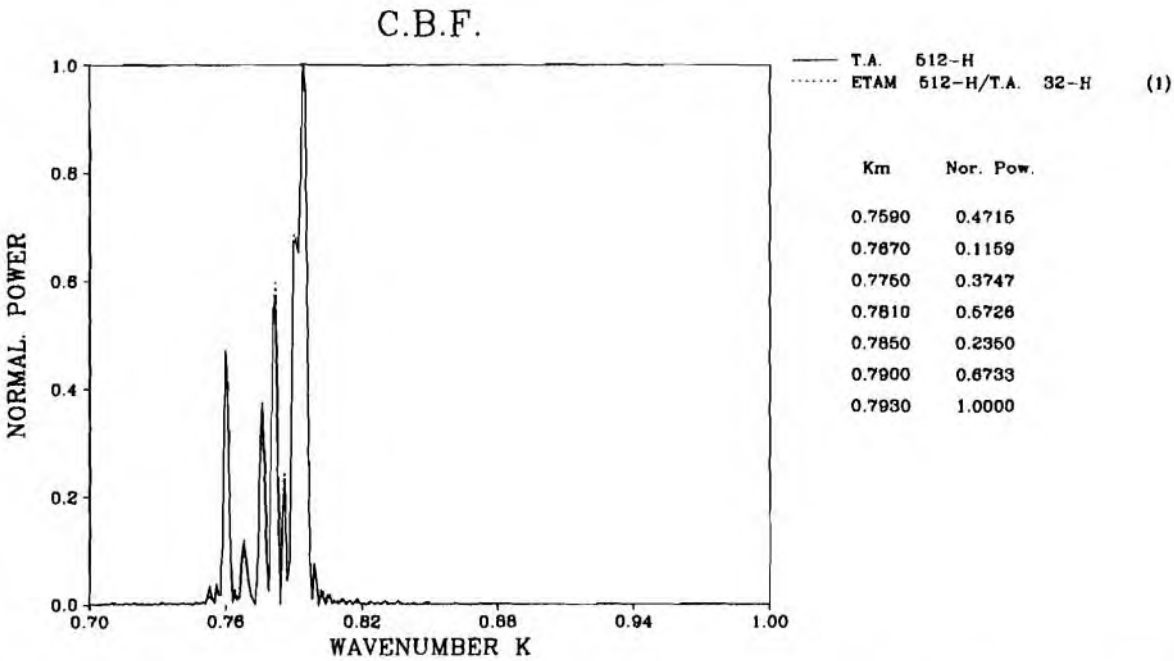

Fig. 5. Recovery of the horizontal wavenumbers k_m shown in Fig. 1 by applying the CBF beamforming technique on synthetic data (a) from a 512 hydrophone towed array (solid curve) and (b) 512 extended towed-array measurements composed from a 32 hydrophone moving towed array (dashed line). The SNR is 20 dB. The numbers on the right are the values of k_m obtained by using a threshold on the normalized power to separate the background noise.

It is appropriate at this point to examine which one of the well-known beamforming techniques best exploits the extended towed-array samples.

The conventional beamformer (CBF) is given by

$$S_{\mathrm{CBF}}(k) = d_n^{\dagger}(k) R_{\mathrm{PP}} d_n(k), \tag{11}$$

where

$$d_n(k) = \exp[-jkr_n], \quad n = 1, 2, \ldots, (N + Jq),$$

$d_n(k)$ is the direction vector, and R_{PP} the crosscorrelation matrix of the space samples $P(r_n, z, \omega_0)$.

The maximum likelihood beamformer (MLM) is given by

$$S_{\mathrm{MLM}}(k) = \frac{1}{d_n^{\dagger}(k) R_{\mathrm{PP}}^{-1} d_n(k)}. \tag{12}$$

For the maximum entropy method (MEM) we have applied the Marple [19] algorithm which has improved performance compared to Burg's [20] pioneering formulation.

It has been shown by many studies [21,22] that for a single source the high-resolution methods (i.e. MLM, MEM) do not provide more accurate spectral estimates than the conventional beamformer (CBF). To achieve high resolution, however, it is necessary to extrapolate the crosscorrelation matrix of the hydrophone space samples beyond the array aperture. The crosscorrelation estimates are known within the towed-array aperture, and any attempt to extrapolate these measurements using MEM requires very good signal-to-noise ratio. This point is illustrated in Fig. 6, where the MEM (i.e. Marple's algorithm) has been applied on the same set of synthetic data shown in Fig. 5. In Fig. 6, however, we have random noise added to the synthetic data and it is apparent from the estimates of the k_m spectrum that the MEM deteriorates in performance as the signal-to-noise ratio becomes small.

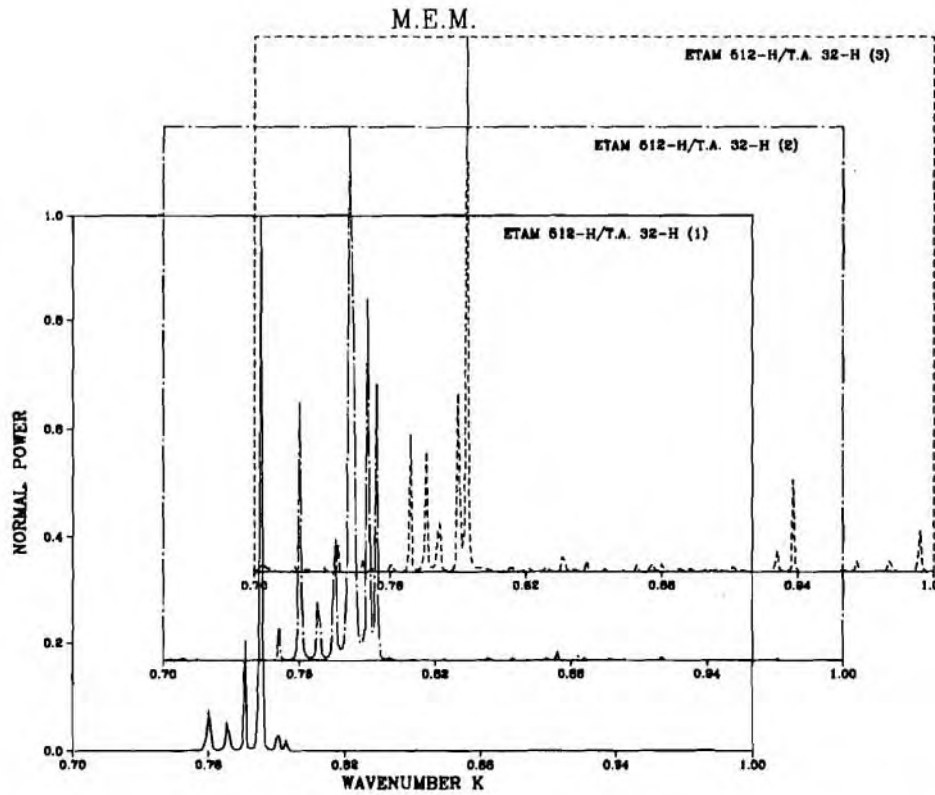

Fig. 6. **Estimates of the horizontal wavenumbers k_m by using the MEM beamforming technique on 512 extended towed-array space samples. The three different curves are for values of SNR: 20 dB, 0 dB and −20 dB.**

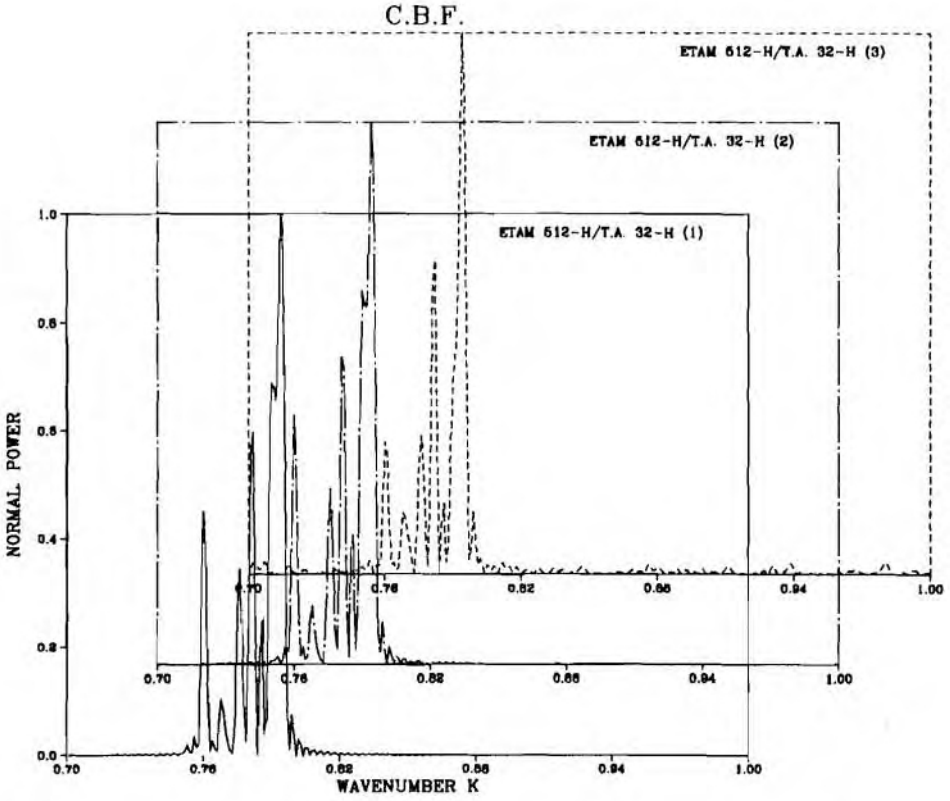

Fig. 7. Estimates of the horizontal wavenumbers k_m by using the CBF beamforming technique on 512 extended towed-array space samples. The three different curves are for values of SNR: 20 dB, 0 dB and −20 dB.

Figure 7 shows the results of the CBF applied to the same set of data as in Fig. 6. As one can see, the CBF has a robust and stable behavior, and it provides very good results up to levels of 0 dB signal-to-noise ratio.

Attempts were made to apply the MLM to our extended towed-array samples. The inversion, however, of the crosscorrelation matrix R_{PP}, using various methods (i.e. eigenvalues/eigenvectors, gauss method) was not possible for matrix sizes larger than 64×64. Even for a 4×4 matrix we had to add noise in its diagonal terms for stabilization in order to be inverted. The main reason for this ill-conditioning of the crosscorrelation matrix is related to the measurements taken at endfire of the towed array that produce an ill-posed matrix.

It is apparent from the above results that the CBF is the best beamformer to recover the k_m spectrum from the extended towed-array samples. An additional comparison

of Fig. 2 with that of Fig. 7 reveals that the CBF provides very good estimates not only for the recovered wavenumbers but also for their relative amplitudes.

3.2. ERROR ANALYSIS

In real data, noise can dominate the measurements such that the signal is barely detectable. Therefore, the results appearing in Fig. 7 should be considered as optimistic.

■ *3.2.1. Random noise*

We have chosen to model the random noise by adding uncorrelated gaussian complex numbers with zero mean and standard deviation σ_A to the synthetic data in Eq. (1). We define the signal-to-noise ratio SNR as

$$\mathrm{SNR} = \frac{\max[P(r_{ln}, z, t_{li})]}{\sigma_{A_l}(t_{li})}. \tag{13}$$

The gaussian noise causes random amplitude fluctuations, causing, in turn, random phase fluctuations in the term $\exp[-j\omega t_{li} + \Delta_\phi]$, where the parameter Δ_ϕ is considered a random variation in the phase term with zero mean and σ_ϕ standard deviation. In addition, in order to quantify the phase fluctuation effects caused by the relative motion between the source and the receiver, we have used a random number generator to create synthetic phase variations in the term $\exp[-j\omega t_{li} + \Delta_{\phi_l}]$ of Eq. (1), where Δ_{ϕ_l} is the standard deviation of the random phase fluctuations in rad with zero mean. Thus, the variance of the phase is $(\sigma_\phi{}^2 + \sigma_{\phi_l}{}^2)$.

Hence, the random noise effects are included in the generated synthetic data of Eq. (1) as random phase variations expressed by $\epsilon(0, \sigma_{\phi_l})$ and as random amplitude fluctuations by $\epsilon(0, \sigma_{A_l}(t_{li}))$.

■ *3.2.2. Towed-array placement errors*

The random placement errors in the expected position of the towed array are caused by random variations in the vector value of speed and by random internal currents. We consider that in practice the maximum integration period of the extended towed-array measurements could be 10–15 min, as has been shown for a deep ocean by recent experimental studies [17]. At the time we start the extended towed-array processing (i.e. $l = 0$), the speed will be v_0, which we call the starting value. During the integration period of 15 min, random errors could start accumulating in the value of v_0. In our study, a typical value for τ is 10–12 s. Therefore, for every interval τ an error in the value of speed will be assumed and expressed by

$$v(\tau_l) = v_0 + \epsilon(0, \sigma_v(\tau_l)), \quad l = 1, 2, \ldots, J. \tag{14}$$

This error in v will induce a placement error in the expected position of the towed array which will be accumulated at every interval τ_l so that

$$r_{ln} = r_0 + (lq + (n-1))d + \sum_{l=1}^{J} \epsilon(0, \sigma_v(\tau_l))\tau, \quad l = 1, 2, \ldots, J. \tag{15}$$

In Eq. (15) the term $\sum_{l=1}^{J} \epsilon(0, \sigma_v(\tau_l))\tau$ gives the random placement error for the expected position of the towed array. It has a minimum value at $l = 0$ and during the time interval $J\tau$ reaches a maximum value.

In addition to the random placement errors, we may have systematic errors caused by an oscillatory course around an assumed straight-line course that the tow ship could have. For this type of systematic error we have

$$\delta r_{ln} = \int_{l\tau}^{(l+1)\tau} v_x(\tau_l)\, \mathrm{d}t, \tag{16}$$

where $v_x(\tau_l) = \sqrt{v_0^2 - v_y^2(\tau_l)}$, $v_y(\tau_l) = v_0 \sin\gamma \cos(2\pi t/T_0)$ (γ is the deviation angle from the straight-line course, T_0 the period of the oscillatory course). Hence, the parameters that determine the systematic placement errors are γ and T_0.

■ *3.2.3. Effects of coherence*

The major concern in dealing with synthetic aperture measurements is the space and time stability or coherence of a narrowband acoustic signal in an underwater environment. Results of experimental studies [23,24] related to this problem have been considered in the formulation of our numerical experiment as discussed above.

In another numerical study [15] the coherence effects were modeled by simply assuming that the signal coherence falls off exponentially with time. Experimental results [23], however, indicate that the coherence variations of the acoustic signal do not follow a smooth decaying process but rather an erratic variation. More specifically, for a passive system the coherence variations may be caused by changes of frequency of the received signal, which are mainly the result of relative movements between the source and receiver, propagation effects, and machinery variations.

Further experimental results [25] concerning the space and time stability of a narrowband acoustic signal have also indicated that the bandwidth of the signal is wide (i.e. 40 mHz) for short ranges (i.e. 18 n.mi) and very small (i.e. 5 mHz) for long ranges (i.e. 60–500 n.mi). This variation in the bandwidth is the result of a shift in frequency, caused probably by bottom reflections at short ranges. In the same study, other sets of results present received signal spectra over an approximate period of 800 s and demonstrate very good coherence levels. This period of 800 s has been

considered in the numerical experiment to be the integration time of our extended towed-array measurements.

Based on the above experimental results, we have chosen to model the effects of coherence in the following way:

- Including an exponential decay,

$$\exp[-l\tau/T_c] \tag{17}$$

  where T_c is the coherence period in the amplitude of the signal during the integration period of the extended towed-array processing. This exponential decay reduces the SNR during the integration period.

- Including a linear variation in the frequency of the received signal expressed by

$$\exp\Big[-j\Big((\omega_0 + \tfrac{1}{2}\beta t_{li})t_{li} + \Delta_{\phi_l}\Big)\Big] \tag{18}$$

  where β in (Hz/s) is the acceleration of ω_0.

We assume that ω_0 has zero mean, and very small random fluctuations in frequency are expressed by random phase fluctuations having zero mean and σ_{ϕ_l} (in rad) standard deviation. The above random variation in the phase term together with the linear change in frequency creates an erratic variation in the coherence of the received signal.

Following the above considerations with respect to the types of errors that could be present in real data, our model for synthetic data includes Eq. (1) modified by Eqs. (13), (15–18).

■ *3.2.4. The variance of estimates*

One fundamental question, which has not been discussed yet, is the relation between the variance of the phase correction estimates, the number of overlapped hydrophones in each set of measurements, and the maximum number of repetitions of the measurements, which define the size of the extended towed array.

The estimates of the phase correction factor by the overlapped correlator are given from Eqs. (5) and (6) and are

$$\Psi_y^{l,l+1} = \arg[P_{n_0,l}|P^{\dagger}_{n,l+1}]_y, \quad y = 1, 2, \ldots, M, \tag{19}$$

where M is the number of overlapped hydrophones; $n_0 = q+1, q+2, \ldots, N; n = 1, 2, \ldots, N-q; M = N-q$; and l the lth repetition of set measurements.

Then

$$\bar{\Psi}^1 = M^{-1}\sum_{y=1}^{M} \Psi_y^{1,2}, \tag{20}$$

$$\tilde{\Psi}^2 = M^{-1}\sum_{y=1}^{M}\Psi_y^{2,3} - \tilde{\Psi}^1,$$

$$\tilde{\Psi}^L = \left[M\sum_{y=1}^{M}\Psi_y^{L,L+1} - \sum_{y=1}^{M}\Psi_y^{L-1,L} + \cdots + (-1)^{L-1}\sum_{y=1}^{M}\Psi_y^{1,2}\right]^{-1}. \tag{21}$$

We define $S^l = M^{-1}\sum_{y=1}^{M}\Psi_y^{l,l+1}$.

During the first set of measurements the estimate of variance for $\tilde{\Psi}^1$ is

$$\sigma^2_{\tilde{\Psi}1} = \frac{\text{var}\{\Psi_y^{1,2}\}}{M}\left[1 + 2\sum_{m=1}^{M-1}\frac{M-m}{M}\varrho(m)\right], \tag{22}$$

where $\varrho(m) = \text{correlation}\{\Psi_y^{1,2}, \Psi_{y+m}^{1,2}\} = d(m)/d(0)$, $d(m) = \text{covariance}\{\Psi_y^{1,2}, \Psi_{y+m}^{1,2}\}$ $d(0) = \text{var}\{\Psi_y^{1,2}\}$, we assume that $\text{var}\{\Psi_y^{1,2}\} = \sigma^2_{\Psi}$. Then for $\varrho(m) = 0$, which indicates that the estimates of $\Psi_y^{1,2}$ are uncorrelated, we have from Eq. (22)

$$\sigma^2_{\tilde{\Psi}1} = \sigma^2_{\Psi}/M. \tag{23}$$

The above expression shows that the variance of $\tilde{\Psi}^1$ is reduced as the overlap sample size becomes large. For highly-correlated estimates of $\Psi_y^{1,2}$ (i.e. $\varrho(m) = 1$) we have

$$\sigma^2_{\tilde{\Psi}1} = \sigma^2_{\Psi}, \tag{24}$$

which demonstrates, as expected, that there is no improvement of the variance of $\tilde{\Psi}^1$ by increasing the overlap size.

The next step is to examine the growth of variance $\sigma^2_{\tilde{\Psi}1}$ caused by the repetition of set measurements during the integration of the extended towed-array processing. In Eq. (21) we have the estimate of $\tilde{\Psi}^L$ for the last Lth repetition as a function of past measurements $\Psi_y^{1,2}, \ldots, \Psi_y^{L,L+1}$. Then the $\text{var}\{\tilde{\Psi}^L\}$ is given from

$$\sigma^2_{\tilde{\Psi}L} = \left[\sum_{l=1}^{L}\text{var}\{S^l\} + 2\sum_{l=1}^{L}(-1)^{l-1}\sum_{m=1}^{L}(-1)^{m-1}\varrho\{S^l, S^m\}\sigma_{S^l}\sigma_{S^m}\right], \quad \text{for } l \neq m. \tag{25}$$

Assuming random variables with $\varrho(m) = 0$ and $\varrho\{S^l, S^m\} = 0$, we have

$$\sigma^2_{\tilde{\Psi}L} = \sigma^2_{\Psi}L/M, \tag{26}$$

where L is the number of iterations and M the sample size on the overlap in terms of number of hydrophones. The above expression shows the control of growth of the

variance $\sigma^2_{\tilde{\Psi}L}$ by the size M of the overlap and the growth of $\sigma^2_{\tilde{\Psi}L}$ with L. Hence, for the uncorrelated case the problem reduces to a random walk.

In the case where the assumption about the noise in Eq. (10) is not valid and $\varrho(m) = 1$, we have from Eqs. (22) and (25) assuming $\varrho\{S^\lambda, S^m\} = 0$,

$$\sigma^2_{\tilde{\Psi}L} = L\sigma^2_{\tilde{\Psi}}. \tag{27}$$

In other words, the growth of variance of $\tilde{\Psi}^L$ is proportional to the number L of repetitions required for the desired size of extended towed-array measurements when the estimates of phase correction factor $\Psi^{l,l+1}_y$ are highly correlated.

4. Results

We have simulated the far field acoustic pressure measurements according to the parameters of the numerical experiment described earlier. A typical record of these measurements is shown in Fig. 8, which includes the numerical signal and its power spectrum for SNR = −20 dB. The effects of the random noise on the recovered wavenumber spectrum of k_m are shown in Fig. 7 for SNR = 20 dB, 0 dB, −20 dB. The good performance of the overlapped correlator for pressure measurements having random noise is expected, based on the discussion in the previous section about the effects of uncorrelated noise on the variance of the phase correction factor.

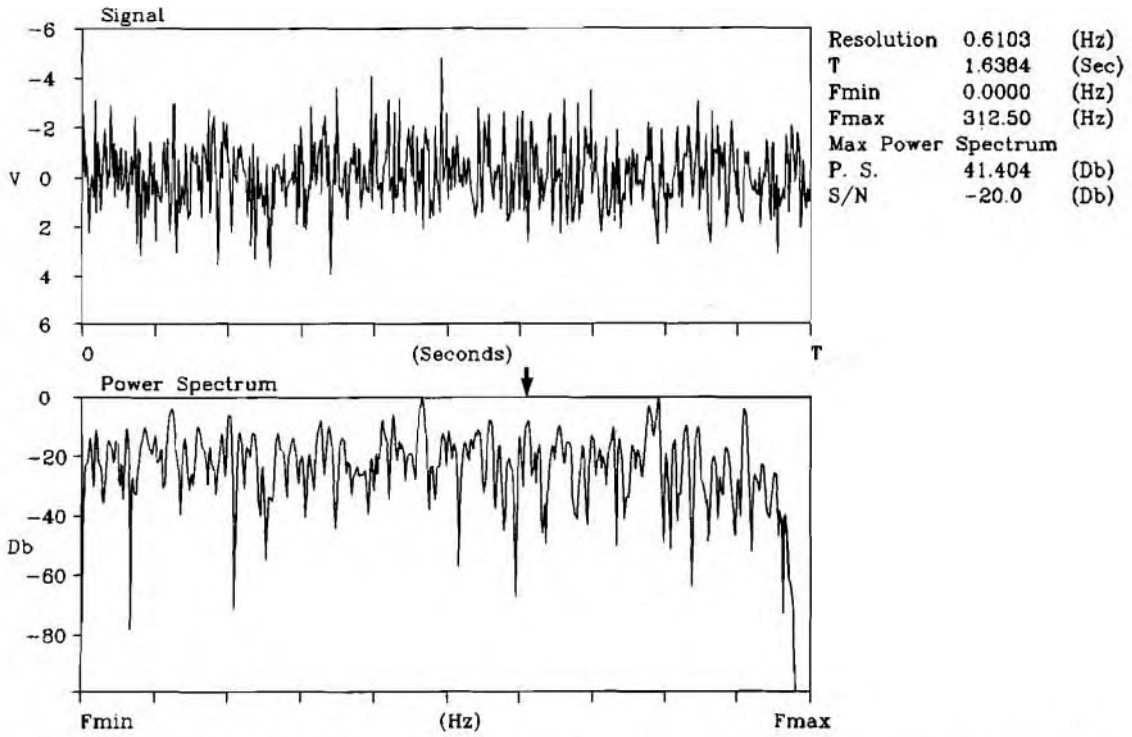

Fig. 8. **Shown in the upper part is the synthetic pressure time signal received by the hydrophones of the towed array. In the lower part the power spectrum of the above signal is shown for SNR = −20 dB. The arrow indicates the frequency component (i.e. 190 Hz) selected through a rarrow numerical band pass filter for beamforming.**

Presented in Fig. 9 are the results of the recovered k_m spectrum for records with coherence period $T_c = 1,\ 0.5,\ 0.12\ T_s$, where T_s is the integration period of the extended towed-array processing. The coherence period, according to Eq. (17), introduces an exponential decay in the signal and affects the value of SNR during the integration period of the extended towed-array processing. So the results in the above figure for $T_c \geq 0.5\,T_s$, which correspond to an average value of SNR of about -10 dB, are in agreement with those of Fig. 7; and the overlapped correlator, as expected, has very poor performance for $T_c = 0.12\,T_s$, since the average value of SNR is -40 dB.

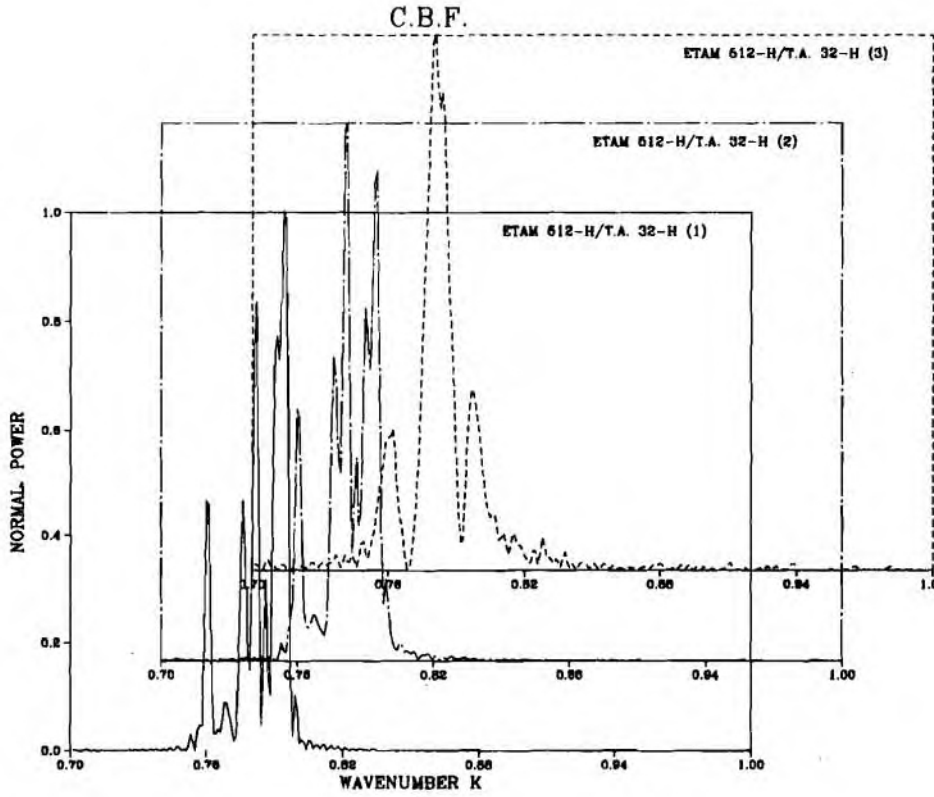

Fig. 9. Estimates of the horizontal wavenumbers k_m from 512 extended towed-array space samples having SNR = 0 dB, using the CBF. The three different curves are for values of coherence period: (1) $T_c = 1T_s$; (2) $T_c = 0.5T_s$; (3) $T_c = 0.12T_s$.

The influence of placement errors of the towed array, caused by random variations of the ship's speed on the recovered k_m spectrum, is shown in Fig. 10. The placement errors are described by Eqs. (14) and (15). The three different curves in the figure are

for maximum random variations in the ship's speed Δv_{max} = 3, 6 and 10% during the integration period of the extended towed-array processing. In this numerical experiment T_s = 820 s and the time interval between two sets of measurements is τ = 12.8 s. In other words, the random variations in the ship's speed, included in the results of Fig. 10, have starting values of Δv_s =0.5, 1 and 2%. At each time interval of τ = 12.8 s when a new random variation is considered then it is accumulated as placement error in the expected position of the towed array. In this way, during the extended towed-array processing, a maximum placement error occurs in the expected position of the actual array. It is important also to note that we do not need to have the actual speed of the towed array equal to a desired value when we start the series of set measurements for the extended towed-array processing. It is clear from Fig. 10 that the overlapped correlator deteriorates in performance as the ship's speed has maximum random variations larger than 8% during the integration period of 820 s. It is expected, however, that at sea-state 3 the random variations in the ship's speed could be smaller than 5% for the time interval of 15 min.

The effects of systematic placement errors, as described by Eq. (16), on the estimates of k_m are presented in Fig. 11. The values of related parameters, in the data of the above figure, of the tow ship's oscillatory course are γ =4°, which is the deviation angle from the straight-line course and T_0 = 8, 1 and 0.12 T_s where T_0 is the period of the oscillatory motion. Clearly from these results one could see that the oscillatory course of the tow ship has very small effect on the estimates of k_m. This would be expected, however, since the source is at the end fire of the towed array; and it has been shown by many investigators that the complications in the towed-array measurements, caused by an oscillatory course of a tow ship, arise mainly when the source is at the broadside of the array.

Our main concern in this numerical study was the time coherence of the received signal for the rather long period of 15 min, which was the integration period of the extended towed-array processing. As discussed in Subsect. 3.2.3, we consider that an appropriate model for the effects of coherence is one that includes a linear variation in the frequency of the source and a random phase term which creates an erratic variation in the coherence of the received signal. It is apparent that a linear variation of the frequency of a source would deteriorate very drastically the coherence of the received signal. In real data [25], however, linear variations of frequency resulting from relative movement between source and receiver quite often are smaller than 0.5 Hz. Presented in Fig. 12 is the recovered spectrum of k_m for 256 hydrophones extended towed-array measurements, for linear variation of frequency βT_s = 0.6 Hz and for SNR = 17 dB, 0 dB. Clearly, the overlapped correlator provides results when the frequency of a source has a very small linear variation and only for very high values of SNR. For numbers larger than 256 (i.e. 512) the recovered spectrum of k_m is very noisy. This poor performance of the overlapped correlator for measurements having variation in the frequency of the source signal is due to the fact that our assumption in Eq. (6) about uncorrelated estimates of the phase correction factor is not valid. In other words, periodic or linear variations in

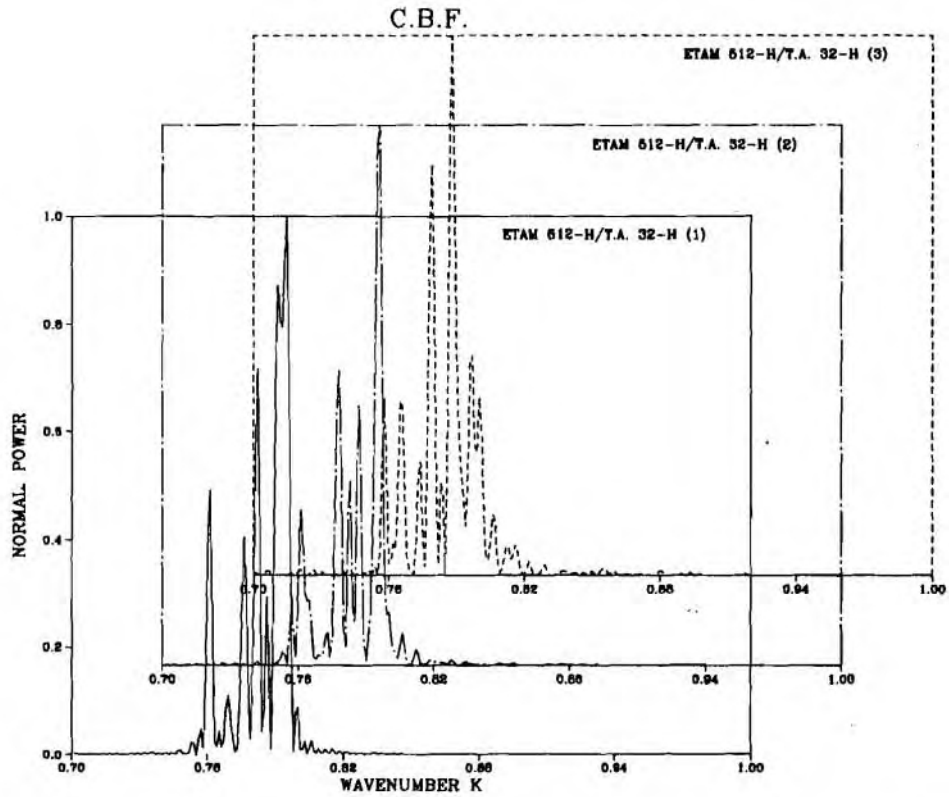

Fig. 10. Estimates of the horizontal wavenumbers k_m from 512 extended towed-array space samples having SNR = 0 dB, using the CBF. The three different curves are for values of maximum random variations of tow ship's speed during the integration period of 14 min: (1) $\Delta v_{max} = 3\%$; (2) $\Delta v_{max} = 6\%$; (3) $\Delta v_{max} = 10\%$.

the frequency of the source indicate that in Eq. (25) the $\varrho\{S^l, S^m\} \neq 0$ and one needs to model the variations of $\bar{\Psi}^l$ to achieve better results. The performance, however, of the overlapped correlator is better when a random phase term is considered. Shown in Fig. 13 are the estimates of k_m for SNR = 0 dB, σ_{ϕ_l} =0.5, 1.0 and 1.5 rad and 512 extended towed-array measurements. Hence, it can be seen that for $\sigma_{\phi_l} \leq 1.5$ rad and rather poor SNR = 0 dB the estimates of k_m are in agreement with the expected values.

From the previous discussion, any variation in the frequency of the source could increase the bandwidth of the received signal. The effects of the bandwidth on the recovered spectrum of k_m are presented in Fig. 14, where SNR = 0 dB and the bandwidth is 50, 100, and 500 mHz. Apparently, for large bandwidth ($\geq$ 100 mHz) we

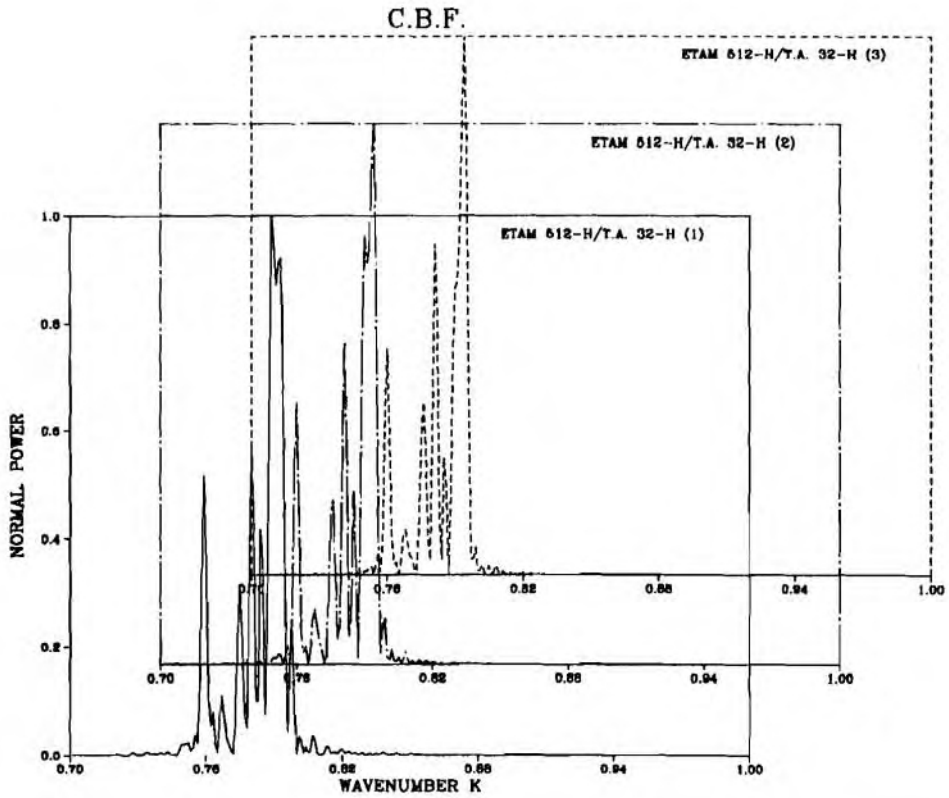

Fig. 11. Estimates of the horizontal wavenumbers k_m from 512 extended towed-array space samples having SNR = 0 dB, using the CBF. The three different curves are for values of $\gamma = 4°$ deviation angle from the assumed straight-line course of the tow ship and periods of the oscillatory course: (1) $T_0 = 8\,T_s$; (2) $T_0 = 1\,T_s$; (3) $T_0 = 0.12\,T_s$.

have sidelobes introduced in the recovered spectrum of k_m. Application of windows on the space samples before beamforming could drastically reduce the sidelobes. The use of windowing, however, will reduce the resolution provided by the large aperture of the extended towed array and, therefore, is not recommended.

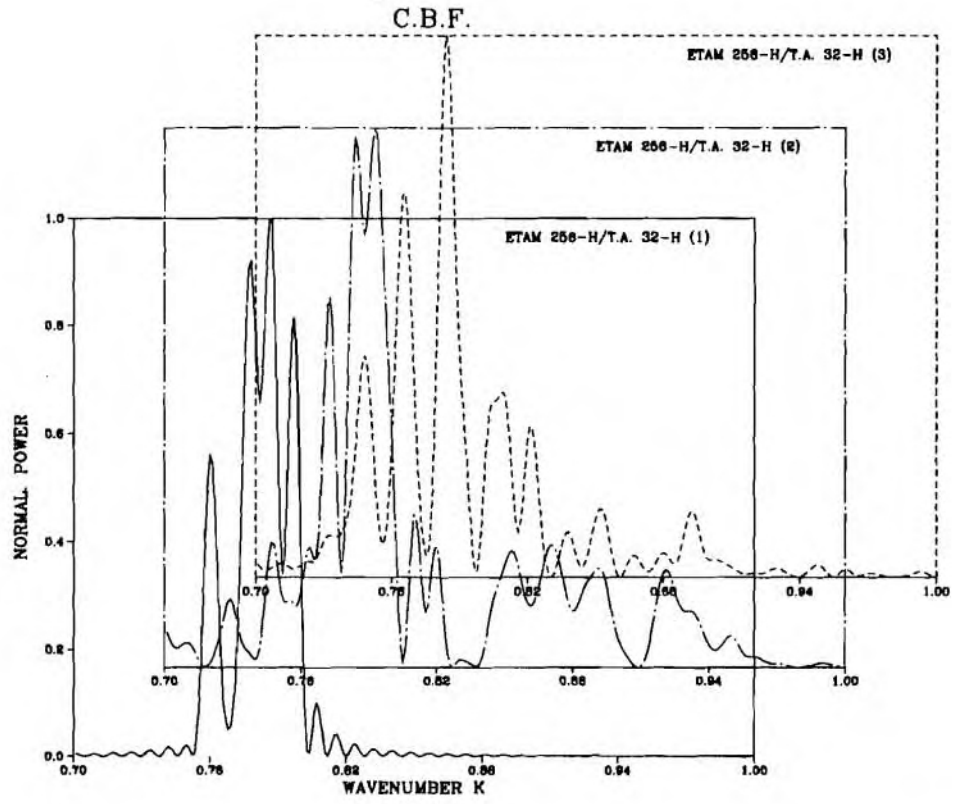

Fig. 12. Effects of linearly varying frequency of a source on the recovered horizontal wavenumbers k_m from 256 extended towed-array space samples using the CBF. The three different curves are for parameters: (1) $\beta T_s = 0$, SNR = 17 dB; (2) $\beta T_s = 0.6$ Hz, SNR = 17 dB; (3) $\beta T_s = 0.6$ Hz, SNR = 0 dB.

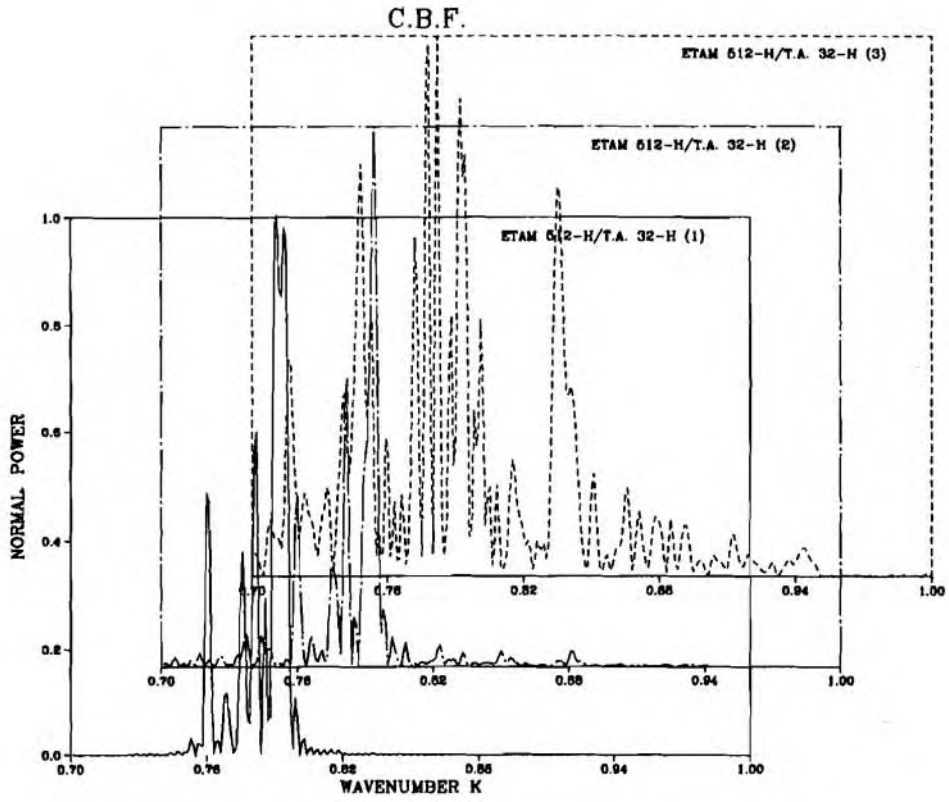

Fig. 13. Effects of random phase variations on the recovered horizontal wavenumbers k_m from 512 extended towed-array space samples using the CBF. The three different curves are for parameters: (1) $\sigma_{\Phi_l} = 0.5$ rad, SNR = 0 dB; (2) $\sigma_{\Phi_l} = 1.0$ rad, SNR = 0 dB; (3) $\sigma_{\Phi_l} = 1.5$ rad, SNR = 0 dB.

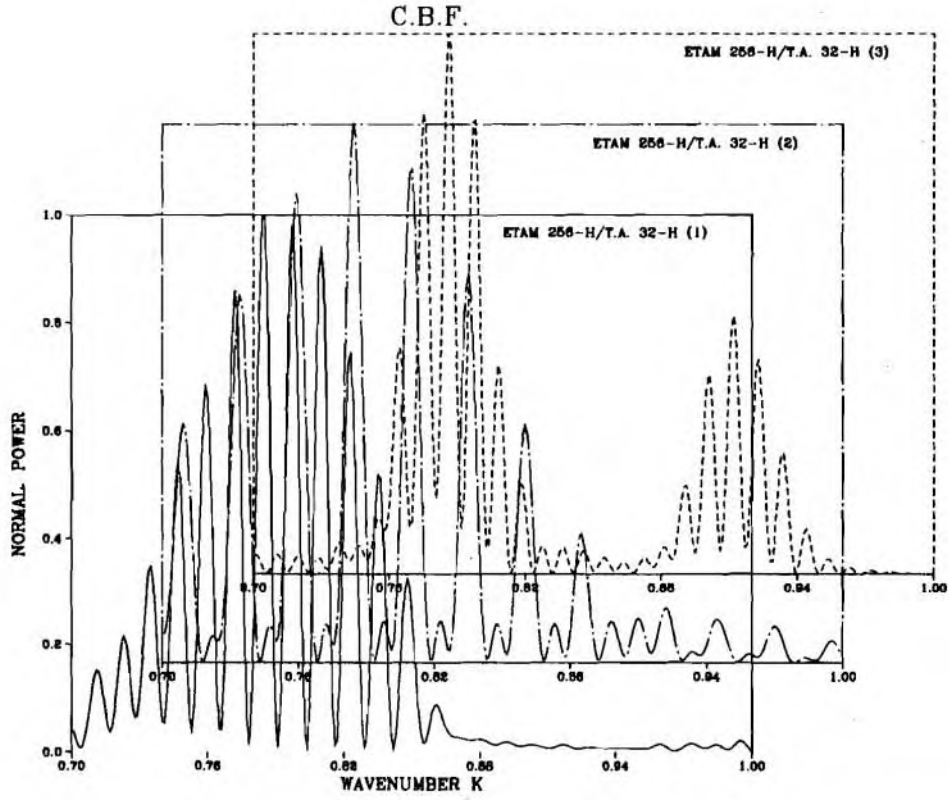

Fig. 14. **Effects of the bandwidth of received signal on the recovered horizontal wavenumbers k_m from 256 extended towed-array space samples having SNR = 0 dB using the CBF. The three different curves are for bandwidth: (1) 50 mHz; (2) 100 mHz; (3) 500 mHz. The expected spectrum of k_m for this case is given in Fig. 12 by the curve (1).**

5. Conclusion

One of the main advantages provided by the overlapped correlator over previous techniques is the following: for the estimates of the phase correction factor $\tilde{\Psi}^l$ there is no need to know the source frequency. The importance of this advantage is shown in Fig. 15, where the spectrum of k_m is recovered from synthetic towed-array measurements having SNR = 0 dB, $\tilde{\Psi}^l = \tilde{\omega}\tau$, $N - q = 0$ (i.e. no overlap) and $\tilde{\omega}$ is different by 0.01 Hz (i.e. 0.005%) from the frequency of the source. Here it is seen that apparently negligible difference in $\tilde{\omega}$ from the expected value ω_0 generates a very noisy spectrum of k_m and it is not possible to recover the wavenumbers. This situation worsens when the previously discussed error effects are included.

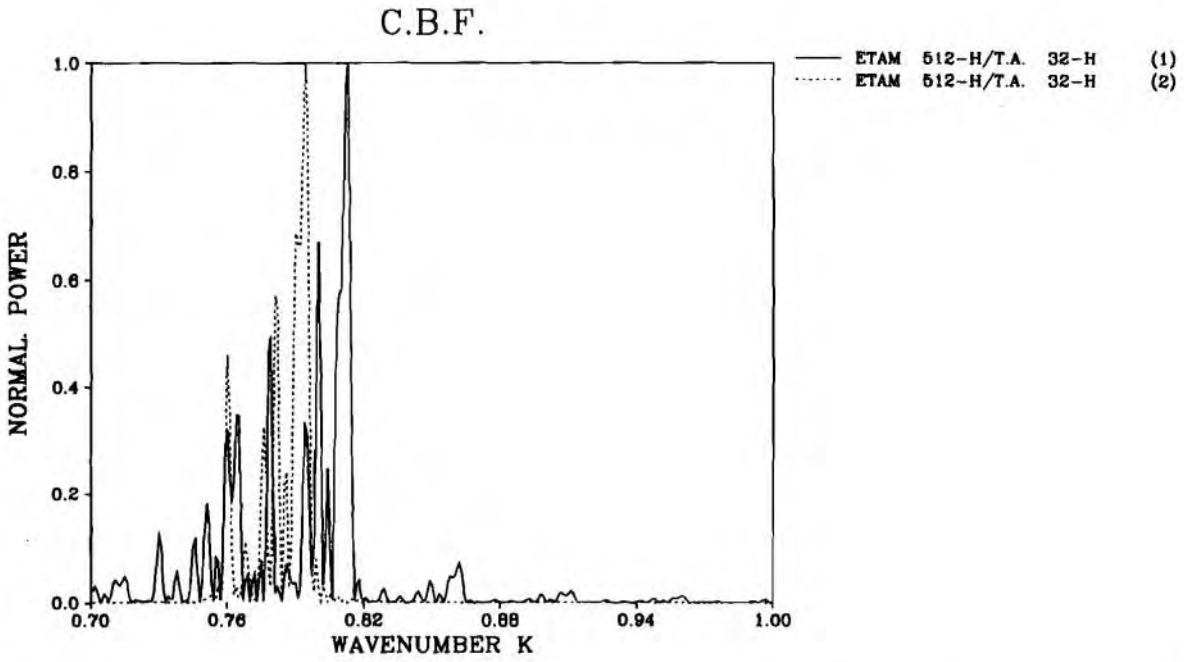

Fig. 15. **Estimates of the horizontal wavenumbers k_m, using the CBF, from 512 extended towed-array space samples having SNR = 0 dB, $N - q = 0$ (i.e. no overlap) and the estimates of the phase correction factor are given by $\tilde{\Psi}^l = \tilde{\omega}\tau$ and not by the overlapped correlator. The value of $\tilde{\omega}$ is different by 0.01 Hz from the expected value of ω_0. The expected spectrum for this case is given in Fig. 5 or by the dashed line (2) in this figure, which is equivalent to curve (2) of Fig. 7.**

Following the examination of the effects of each type of errors on the recovered spectrum of k_m one may ask what would be the situation when all these types of errors appear in one record of extended towed-array samples. We consider that the magnitudes of the parameters describing the different types of errors, which may appear in a real experiment with sea state smaller than 3, are as follows:

- The SNR of the received signal is 0 dB.
- The maximum random variations in the tow-ship's speed, during the integration period of 15 min, is 5%.
- The coherence period, as defined in Eq. (17), is $T_c \approx 800$ s. Experimental observations indicate that T_c could be longer than 800 s.
- Oscillatory course of the tow ship, caused by the influence of winds and currents, could be well controlled and we expect to have $\gamma = 2°$ take-off angle and $T_0 \approx 800$ s for 80 m long tow ship and speed 4–5 kn.
- Random phase fluctuations σ_{Φ_l} are in the range of 1.0–1.5 rad.

Presented in Fig. 16 are the recovered wavenumbers k_m from 512 hydrophone extended towed-array samples and for the above error parameters. Apparently the estimated wavenumbers agree with the expected values in Fig. 1. In the case a variation in the frequency of the source is considered, as defined by Eq. (18), the SNR has to be larger than 15 dB to have good estimates of k_m.

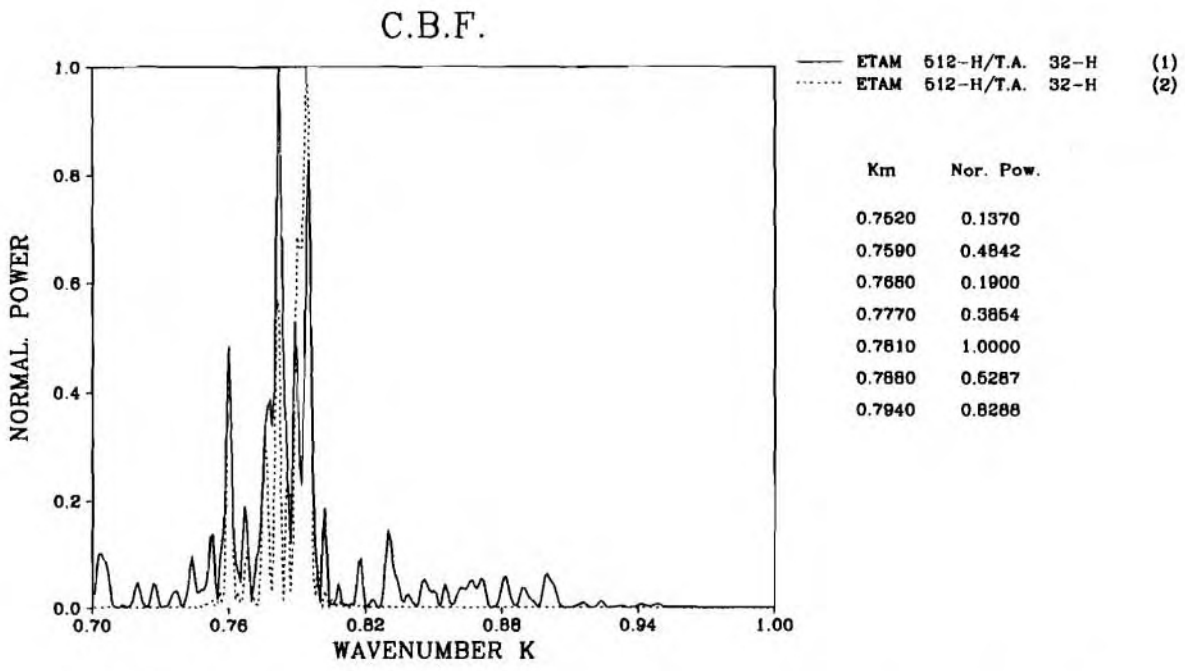

Fig. 16. Estimates of the horizontal wavenumbers k_m, using the CBF, from 512 extended towed-array space samples having: curve (1) – SNR = 0 dB, $T_c = 1T_s$, $T_0 = 1T_s$, $\gamma = 2°$, $\Delta v_{max} = 5\%$, $\sigma_{\phi_l} = 1.0$ rad. The curve (2) has SNR = 0 dB, all the error parameters very negligible and it is equivalent to the curve (2) in Fig. 7. The numbers on the right-hand side of this figure are the recovered wavenumbers k_m from its curve (1) and are in very good agreement with those of Fig. 5.

References

[1] BUCKER, H.P. Use of calculated sound fields and matched-field detection to locate sound sources in shallow water. *Journal of the Acoustical Society of America*, **59**, 1976: 368–373.

[2] HINICH, M.J. Maximum likelihood estimation of the position of a radiating source in a waveguide. *Journal of the Acoustical Society of America*, **66**, 1979: 480–483.

[3] HINICH, M.J. and SULLIVAN, E.J. Maximum-likelihood passive localization using mode filtering. Submitted to the *Journal of the Acoustical Society of America*, 1988.

[4] YANG, T.C. A method of range and depth estimation by modal decomposition. *Journal of the Acoustical Society of America*, **82**, 1987: 1736–1745.

[5] HINICH, M.J. Array design for measuring source depth in a horizontal waveguide. *SIAM Journal on Applied Mathematics*, **32**, 1977: 800–806.

[6] SULLIVAN, E.J. Passive localization using propagation models. SACLANTCEN SR-117. La Spezia, Italy, SACLANT Undersea Research Centre, 1987.

[7] BAGGEROER, B., KUPERMAN, W.A. and SCHMIDT, H. Performance bounds on array processing for source localization using full wave modeling of signal and noise fields. *In* : LEE, D., STERNBERG, R.L. and SCHULTZ, M.H., *eds.* Computational Acoustics, Algorithms and Applications. Proceedings of the 1st IMACS Symposium, New Haven, CT, 6–8 August 1986, volume 2. Amsterdam, North-Holland, 1988: pp. 299–319.

[8] SULLIVAN, E.J. and RAMEAU, K. Passive ranging as an inverse problem: A sensitivity study. SACLANTCEN SR-118. La Spezia, Italy, SACLANT Undersea Research Centre, 1987.

[9] SHANG, E.C., CLAY, C.S. and WANG, Y.Y. Passive harmonic source ranging in waveguides by using mode filter. *Journal of the Acoustical Society of America*, **78**, 1985: 172–175.

[10] KLEMM, R. Range and depth estimation by line arrays in shallow water. *Signal Processing*, **3**, 1981: 333–344.

[11] SHANG, E.C., WANG, H.P. and HUANG, Z.Y. Waveguide characterization and source localization in shallow water waveguides using the PRONY method. *Journal of the Acoustical Society of America*, **83**, 1988: 103–108.

[12] CANDY, J.V. and SULLIVAN, E.J. Model based passive ranging. Submitted to the *Journal of the Acoustical Society of America*, 1988.

[13] FRISK, G.V. and LYNCH, J.F. Shallow water waveguide characterization using the Hankel transform. *Journal of the Acoustical Society of America*, **76**, 1984: 205.

[14] WILLIAMS, R.E. Creating an acoustic synthetic aperture in the ocean. *Journal of the Acoustical Society of America*, **60**, 1976: 60–73.

[15] PUSONE, E.G. and LLOYD, L.J. Synthetic-aperture sonar: performance analysis of beamforming and system design. SACLANTCEN SR-91. La Spezia, Italy, SACLANT Undersea Research Centre, 1985.

[16] BROEK, H.W. Temporal and spatial fluctuations in single-path underwater acoustic wave fronts, I: Transmission from the first convergence zone at 43-n.mi range. *Journal of the Acoustical Society of America*, **72**, 1982: 1527–1532.

[17] WILLIAMS, R.E. and WEI, C.H. Spatial and temporal fluctuations of acoustic signals propagated over long ocean paths. *Journal of the Acoustical Society of America*, **59**, 1976: 1299–1309.

[18] JENSEN, F. and FERLA, M.C. SNAP: The SACLANTCEN normal-mode acoustic propagation model. SACLANTCEN SM-121. La Spezia, Italy, SACLANT Undersea Research Centre, 1979. [AD A 067 256]

[19] MARPLE L. A new autoregressive spectrum analysis. *IEEE Transactions on Acoustics, Speech, and Signal Processing*, **28**, 1980: 441–454.

[20] BURG, J.P. Maximum entropy spectral analysis. Ph.D. dissertation. Stanford, CA, Stanford University, 1975.

[21] ZIMMER, W.M.X. High-resolution beamforming techniques, performance analysis. SACLANTCEN SR-104. La Spezia, Italy, SACLANT Undersea Research Centre, 1986.

[22] WAGSTAFF, R.A. and BERROU, J.-L. A fast and simple nonlinear technique for high resolution beamforming and spectral analysis. *Journal of the Acoustical Society of America*, **75**, 1984: 1133–1141.

[23] WILLIAMS, R.E. and WEI, C.H. The correlation of acoustic wavefronts and signal time-base instabilities in the ocean. *Journal of the Acoustical Society of America*, **59**, 1976: 1310–1316.

[24] MANGANO, D.T. and BROEK, H.W. Correlation of phase and amplitude fluctuations at hydrophones spaced one-half to two wavelengths apart. *Journal of the Acoustical Society of America*, **72**, 1982: 1556–1562.

[25] KOENIGS, P.D., HERSTEIN, P.D. and BROWNING, D.G. Further study of the space and time stability of a narrowband acoustic signal in the ocean: short range results. *Journal of the Acoustical Society of America*, **70**, 1981: S16:H3.

Report no. changed (Mar 2006): SM-214-UU

Initial Distribution for SM-214

Ministries of Defence	
JSPHQ Belgium	2
DND Canada	10
CHOD Denmark	8
MOD France	8
MOD Germany	15
MOD Greece	11
MOD Italy	10
MOD Netherlands	12
CHOD Norway	10
MOD Portugal	5
MOD Spain	2
MOD Turkey	5
MOD UK	20
SECDEF US	60
NATO Authorities	
Defence Planning Committee	3
NAMILCOM	2
SACLANT	3
SACLANTREPEUR	1
CINCWESTLANT/ COMOCEANLANT	1
COMSTRIKFLTANT	1
CINCIBERLANT	1
CINCEASTLANT	1
COMSUBACLANT	1
COMMAIREASTLANT	1
SACEUR	2
CINCNORTH	1
CINCSOUTH	1
COMNAVSOUTH	1
COMSTRIKFORSOUTH	1
COMEDCENT	1
COMMARAIRMED	1
CINCHAN	3
SCNR for SACLANTCEN	
SCNR Belgium	1
SCNR Canada	1
SCNR Denmark	1
SCNR Germany	1
SCNR Greece	1
SCNR Italy	1
SCNR Netherlands	1
SCNR Norway	1
SCNR Portugal	1
SCNR Turkey	1
SCNR UK	1
SCNR US	2
SECGEN Rep. SCNR	1
NAMILCOM Rep. SCNR	1
National Liaison Officers	
NLO Canada	1
NLO Denmark	1
NLO Germany	1
NLO Italy	1
NLO UK	1
NLO US	1
NLR to SACLANT	
NLR Belgium	1
NLR Canada	1
NLR Denmark	1
NLR Germany	1
NLR Greece	1
NLR Italy	1
NLR Netherlands	1
NLR Norway	1
NLR Portugal	1
NLR Turkey	1
NLR UK	1
Total external distribution	236
SACLANTCEN Library	10
Stock	34
Total number of copies	280